THE ASTRONOMICAL JOURNAL VOLUME 113, NUMBER 2 FEBRUARY 1997

STELLAR POPULATIONS IN THE LARGE MAGELLANIC CLOUD: EVIDENCE FOR A SIGNIFICANT NUMBER OF OLDER STARS OR A STEEPER IMF?[1]

JON A. HOLTZMAN,[2] JEREMY R. MOULD,[3] JOHN S. GALLAGHER III,[4] ALAN M. WATSON,[2] CARL J. GRILLMAIR,[5] GILDA E. BALLESTER,[6] CHRISTOPHER J. BURROWS,[6] JOHN T. CLARKE,[7] DAVID CRISP,[5] ROBIN W. EVANS,[5] RICHARD E. GRIFFITHS,[8] J. JEFF HESTER,[9] JOHN G. HOESSEL,[4] PAUL A. SCOWEN,[9] KARL R. STAPELFELDT,[5] JOHN T. TRAUGER,[5] AND JAMES A. WESTPHAL[10]

Received 1996 August 30; revised 1996 November 12

ABSTRACT

We present deep photometry obtained with the *HST* in an outer LMC field. A well-defined main sequence is seen down to $V>26$. We derive a luminosity function from the data and use it to constrain the IMF and the star formation history. We derive limits on the IMF slope, α (with $dN/dM \propto M^{\alpha}$), from stars on the main sequence which are fainter than the oldest turnoff. For most choices of star formation history and metallicity, we derive slopes which are consistent the Salpeter ($\alpha=-2.35$) or local solar neighborhood IMF, although the preferred values are steeper. We can rule out IMF slopes shallower than -1.6 and steeper than -3.1 for the mass range $0.6 \lesssim M \lesssim 1.1\ M_{\odot}$. Assuming a Salpeter IMF over the entire observed mass range, we derive star formation histories from the entire luminosity function, which covers the mass range $0.6 \lesssim M \lesssim 3\ M_{\odot}$. We find that the luminosity function is inconsistent with the scenario in which the bulk of the field stars in the LMC are younger than 4 Gyr. Instead, we find that there must be a comparable number of stars older and younger than 4 Gyr. Our best model has a star formation rate which is roughly constant for 10 Gyr then increases by about a factor of three for the past 2 Gyr. Such a model is also roughly consistent with the distribution of stars in the color-magnitude diagram. Similar model parameters are derived if we adopt the Kroupa, Tout, and Gilmore solar neighborhood IMF instead of a Salpeter slope. Alternatively, we can fit the luminosity function with a predominantly young population if we use a steeper single power law IMF slope with $\alpha \sim -2.75$ over the entire range of observed masses. © *1997 American Astronomical Society.* [S0004-6256(97)03102-6]

1. INTRODUCTION

As the nearest galaxy, the LMC offers an excellent opportunity to study low mass stars in a setting different from that of the Milky Way. The luminosity function of low mass stars is particularly interesting because it can be used to infer the initial mass function (IMF) roughly independently of the star formation history, because low mass stars live longer than a Hubble time on the main sequence. Understanding whether there are variations of the IMF with galaxy type or metallicity is essential to our understanding of star formation. Additionally, if the IMF slope can be extrapolated to higher masses and assumed to be time-independent, the luminosity function of higher mass stars can be used to infer information about the star formation history. In particular, the relative numbers of intermediate and low mass stars on the main sequence provides a constraint on the relative number of old and young stars. A knowledge of the star formation history in different types of galaxies is critical for constraining models of galaxy evolution.

Deep ground-based photometry of LMC field stars has been described by Butcher (1977), Stryker (1984), Bertelli *et al.* (1992), and Vallenari *et al.* (1996a,b), among others (see reviews by Feast 1995 and Mateo 1991). Most of these studies reach a similar conclusion, namely that the bulk of

[1]Based on observations with the NASA/ESA *Hubble Space Telescope*, obtained at the Space Telescope Science Institute, operated by AURA Inc under contract to NASA.

[2]Department of Astronomy, New Mexico State University, Dept 4500 Box 30001, Las Cruces, NM 88003, electronic mail: holtz@nmsu.edu, awatson@nmsu.edu

[3]Mount Stromlo and Siding Spring Observatories, Australian National University, Private Bag, Weston Creek Post Office, ACT 2611, Australia, electronic mail: jrm@mso.anu.edu.au

[4]Department of Astronomy, University of Wisconsin–Madison, 475 N. Charter St., Madison, WI 53706, electronic mail: jsg@jayg.astro.wisc.edu, hoessel@jth.astro.wisc.edu

[5]Jet Propulsion Laboratory, 4800 Oak Grove Drive, Pasadena, CA 91109, electronic mail: carl@wfpc2-mail.jpl.nasa.gov, dc@crispy.jpl.nasa.gov, rwe@wfpc2-mail.jpl.nasa.gov, krs@wfpc2-mail.jpl.nasa.gov, jtt@wfpc2-mail.jpl.nasa.gov

[6]Department of Atmospheric, Oceanic, and Space Sciences, University of Michigan, 2455 Hayward, Ann Arbor, MI 48109, electronic mail: gilda@sunshine.sprl.umich.edu, clarke@sunshine.sprl.umich.edu

[7]Astrophysics Division, Space Science Department, ESA & Space Telescope Science Institute, 3700 San Martin Drive, Baltimore, MD 21218, electronic mail: burrows@stsci.edu

[8]Department of Physics, Carnegie Mellon University, 5000 Forbes Ave, Pittsburgh, PA 15213

[9]Department of Physics and Astronomy, Arizona State University, Tyler Mall, Tempe, AZ 85287, electronic mail: jjh@cosmos.la.asu.edu, scowen@tycho.la.asu.edu

[10]Division of Geological and Planetary Sciences, California Institute of Technology, Pasadena, CA 91125, electronic mail: jaw@sol1.gps.caltech.edu

 0004-6256/97/113(2)/656/13/$10.00

the field stars in the LMC are of intermediate and young age. The most quantitative studies have been done by Bertelli *et al.* and Vallenari *et al.*, who use deep, high quality B and V band CCD observations to photometer LMC field stars. However, even these observations barely reach the turnoff expected for an old population. By analyzing star count data in different regions of the color-magnitude diagrams, they derive preferred star formation histories in several fields around the LMC. Generally, they get reasonable fits using a Salpeter IMF and a star formation history which has low star formation rates until a "burst time," τ_B, when the star formation rate increases by a factor of 5–10. In most of their fields, a burst lookback time of $2<\tau_B<4$ Gyr is preferred, although in a few fields, larger values provide better fits. Their models generally have the bulk of the stars in the LMC field being formed recently. A star formation history with the bulk of the stars formed recently on top of a small component of old stars is also mirrored in the age distribution of rich star clusters in the LMC; a few very old clusters are found with hardly any intermediate age clusters, and then a large number of younger clusters (e.g., Olszewski 1993). However, one might not necessarily expect the field star age distribution to be comparable to that of stellar clusters because clusters may disrupt as time passes.

Direct measurements of the IMF have been made for several LMC clusters. Mateo (1988) presents IMF measurements in six clusters for stars in the range $1\lesssim M\lesssim 10\,M_\odot$ and finds that all the clusters have a similar IMF with a slope of $\alpha\sim -3.5$, where $dN/dM \propto M^\alpha$. In addition, he finds that the LMC cluster IMFs are essentially indistiguishable from the solar neighborhood IMF derived by Scalo (1986). Recent *HST* measurements of the cluster NGC 1818 (Hunter *et al.* 1997), which probe somewhat lower masses, indicate a shallower slope of ~ -2.2.

We have observed a field near the LMC cluster NGC 1866 with the Wide Field Planetary Camera 2 on the *Hubble Space Telescope* in order to observe faint, low mass, stars. This is in the same vicinity as one of the fields analyzed by Bertelli *et al.* (1992). Gallagher *et al.* (1996) presented an analysis of the brighter stars observed in the field based on aperture photometry. By comparing the distribution of stars in the color-magnitude diagram with stellar models that predict lifetimes along evolutionary tracks, they concluded that star formation has been roughly constant over the last few billion years in this field. On top of this roughly constant star formation, they suggest that a small burst in star formation occurred about 2 Gyr ago, the precise age depending on the metallicity. The evidence for this burst is the presence of a subgiant branch in the color-magnitude diagram about a magnitude brighter than the subgiant branch of older stars, although it is unclear whether this represents a local or global variation in the LMC star formation rate.

In this paper we concentrate on the fainter stars and the stellar luminosity function. A careful treatment of the photometric measurements and their errors is used along with detailed modelling of star counts within the color-magnitude diagram to measure the IMF of unevolved stars. We then try to estimate the star formation history of this LMC field from the luminosity function.

2. OBSERVATIONS

Observations of the LMC field were obtained on 1994 May 25 with the Wide Field Planetary Camera 2 of the *Hubble Space Telescope*. Observations were made through the F555W and F814W filters (wide V and I) with a total of 4000s through each filter. Observations through each filter were split into four exposures with exposure times of 600, 1000, 1000, and 1400 seconds. All observations were made with the electronics bay which gives approximately 14 electrons per DN.

The data were processed using the standard reduction techniques discussed by Holtzman *et al.* (1995a, H95A). This processing included a very small correction for analog-to-digital errors, overscan and bias subtraction, dark subtraction, a tiny shutter shading correction, and flat fielding. Unfortunately, this set of images had some bias structure which was not entirely removed by the superbias subtraction, slightly decreasing our sensitivity at faint levels.

2.1 Photometry

Figure 1 shows the combined set of F555W exposures. It can be seen that this is a relatively sparse field, making stellar photometry reasonably uncomplicated. For most of the brightest stars, simple aperture photometry yields excellent results. However, we were interested in pushing the photometry down to the faintest levels so we could measure the IMF of the unevolved main sequence. Consequently, we used profile-fitting photometry since this provides optimal signal-to-noise for the faintest stars.

A model stellar point spread function (PSF) that varies across the field of view was used. The model PSF was derived from a detailed optical study. The optical model incorporates variation of the pupil function across the field of view as determined from the camera design, variation of aberrations across the field of view as determined from phase retrieval of a number of moderately bright stars in a separate field (Holtzman *et al.* 1997), and medium-scale structure on the *HST* mirrors as determined from out-of-focus images taken with WFPC2 (Krist & Burrows 1994). Observed spacecraft jitter information for each of the LMC exposures was incorporated into a model PSF for each exposure. In addition, phase retrieval was performed for several stars in each exposure to determine a separate focus value for each exposure, since the *HST* is known to have small focus variations on orbital time scales. Consequently, the resulting PSF models include time-independent aberration and pupil function variation along with time-dependent jitter and focus. As such, they include several important effects which are not treated, for example, by the TinyTim PSF software. The model PSFs still do not provide perfect matches to the observed profiles, but they rival the quality obtained from other methods of PSF determination. They avoid many of the problems of empirical determinations of the PSF, which suffer from undersampling and the requirement of many stars across the field to model field-dependent PSF variations. In addition, the models include stellar wings and diffraction spikes which are difficult to model empirically because stars which have sufficient S/N to measure these are saturated in

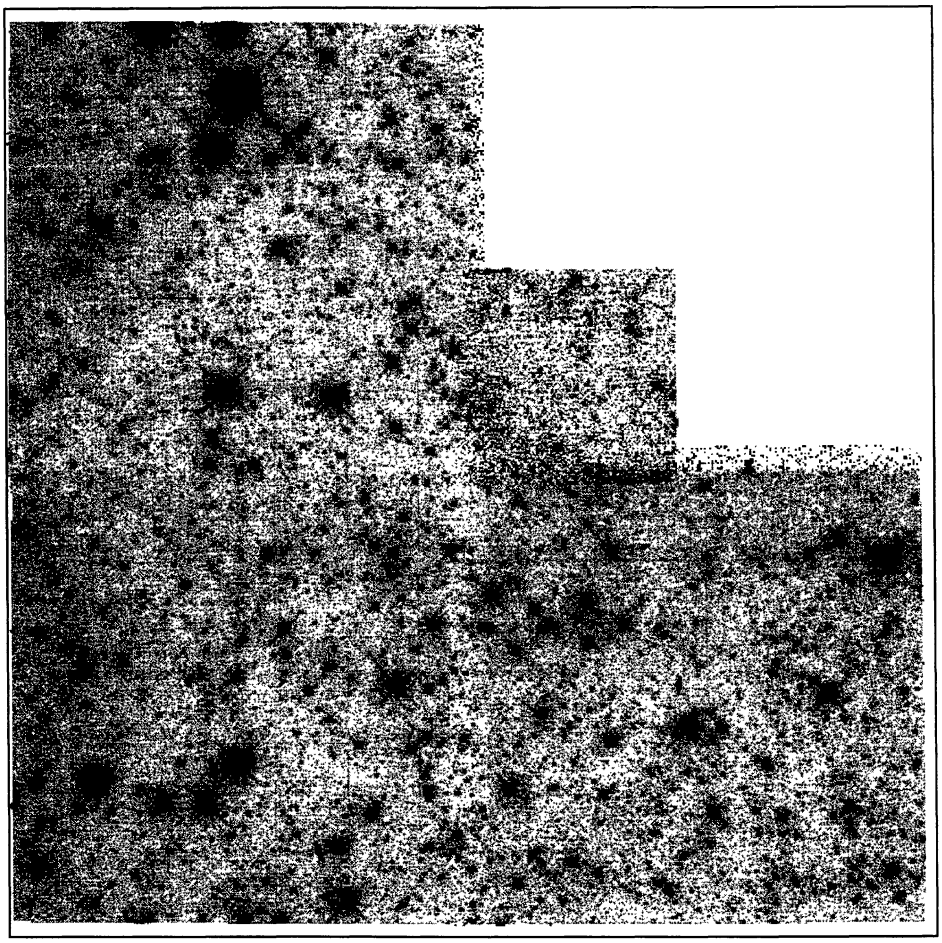

FIG. 1. The WFPC2 F555W image of the LMC field.

their cores. Using these model PSFs leads to noticeable improvements over results obtained using a field-independent observed PSF. The relative quality of the photometry as compared with empirical field-dependent PSFs is difficult to quantify as it depends on how much data are available to make the empirical PSFs and whether these data provide a close match (similar jitter and focus) to the PSFs in the field being reduced.

To perform the profile-fitting photometry, the four frames in each color were first combined to reject cosmic rays based on the known noise properties of the WFPC2 detectors. Since the F555W and F814W frames are approximately equally deep, the combined frames for each filter were summed, and the summed image was used for star detection. Given the input star list, profile fitting was then performed simultaneously on the set of eight individual frames, solving for a brightness for each star in each color, a position for each star, a separate background value for each group of stars in each frame, and frame-to-frame pointing shifts. The simultaneous reduction of all the frames has several advantages over reduction of each frame individually or of the summed CR-rejected frame. First, the physical requirement is imposed that all frames have the same star list with the same relative positions (after allowing for the variation in scale as a function of wavelength as discussed in H95A). Simultaneous reduction of the eight frames also allows a separate PSF to be used for each frame. Since small pointing differences between the frames provide slightly different pixel samplings of the PSF, this provides additional information for fitting the PSF which is undersampled in each of the individual frames. Cosmic rays in each of the individual frames were flagged by the procedure which combined the stack of frames for star-finding, and these pixels were ignored in the profile-fitting procedure.

The profile fitting was iterated three times. On the first pass, only the brightest stars were fit. This allowed subtraction of these stars including the extensive stellar wings and diffraction spikes. The star finding algorithm was then used on the subtracted frames, allowing detection of faint objects without as many spurious detections of objects in the wings of the bright stars. Some constraints were placed on the star finding in this pass to avoid spurious detections around bright stars from imperfect PSF subtraction. The second pass was used to find and fit all of the bright and faint stars. These stars were subtracted, and any close neighbors of stars which were not found on the second pass were detected. These were added to the list of stars, and a final stellar photometry run was made. During each of the profile-fitting stages, the

software attempted to remove spurious detections by deleting stars that were not well fit by the stellar PSF. The final photometry list was filtered once again using a goodness-of-fit index to remove spurious detections which remained.

Subsequent to the profile fitting, aperture photometry was also performed for all of the stars. This was done in conjunction with the profile-fitting results by subtracting all of the stars from the frame, then doing aperture photometry on each individual star after it was added back into the subtracted frame; a similar method has been used by Guhathakurta *et al.* (1996). This provides superior photometry for bright stars, but for the fainter stars the profile fits seem to be more robust as they use optimal weighting and are better able to minimize the effect of deviant pixels arising from close blends, background galaxies, noise spikes, etc. Since we are concentrating on the luminosity function, particularly of the fainter stars, we use the profile results here.

The resulting magnitudes were transformed to the synthetic WFPC2 photometric system defined by Holtzman *et al.* (1995b, H95B). The profile results were converted to instrumental aperture magnitudes with a 0.5 arcsec radius aperture using the aperture photometry of reasonably isolated stars. The aperture corrections were determined by inspecting the difference between the 0.5 arcsec aperture and profile-fitting results; a separate correction was allowed for each of the four chips, although they all agreed to within a few percent. We judge the accuracy of the aperture corrections to be one or two percent in the worst case. The corrected profile fitting results were then put on the WFPC2 system by the application of the zeropoints given in H95B. Because these were fairly long exposures with typically $\sim 35e^-$ background, we made no correction for possible CTE effects, as discussed in H95B; if CTE problems were present they would only change the derived magnitudes by a few percent and our conclusions would be unaffected. No correction was made for a possible systematic effect which may give differences in photometric zeropoint between long and short exposures (see Note Added in Proof, H95B); applying such a correction would make all our magnitudes about 0.05 mag fainter.

We use the WFPC2 synthetic system rather than transforming to V and I because the transformations have some small observational uncertainties and metallicity dependences and we do not know *a priori* the metallicity (which itself may be a function of magnitude, depending on the star formation history). In addition, we believe we have a good understanding of the physical WFPC2 response and filter bandpasses which we need to compute expected colors from stellar models (H95B).

The calibrated color-magnitude diagram is presented in Fig. 2. A well defined main sequence can be seen down to $M_{\mathrm{F555W}} \sim V > 26$.

2.2 Completeness and Error Estimation

To accurately interpret a luminosity function, an understanding of the detection efficiency and measurement errors as a function of stellar brightness is needed. To estimate these, we performed a series of artificial star experiments. In each test, we added a grid of stars of equal brightness onto

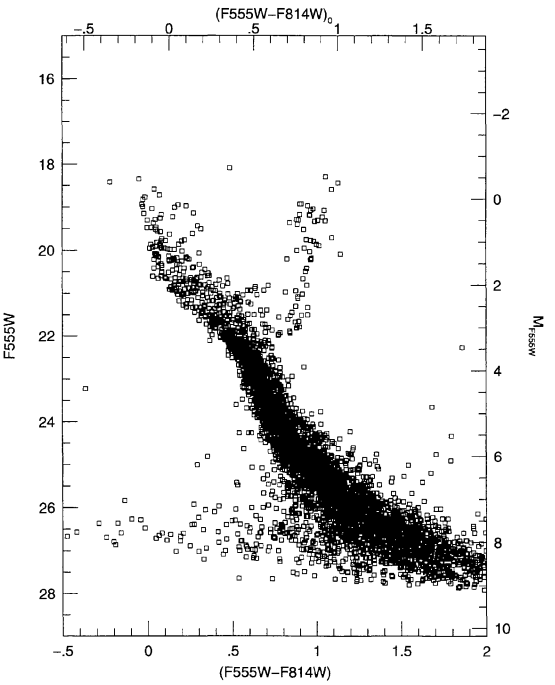

FIG. 2. The color-magnitude diagram obtained from the field.

each exposure in each of the four chips. The grid spacings were chosen to insure that the artificial stars were isolated from each other and thus did not add significantly to the crowding on the frame; we placed 121 stars on the PC, and 529 stars on each of the WFs. The model PSFs were used to place the stars on each frame using the positional information (frame to frame shifts and scale changes) derived from the fitting of the frames without the artificial stars. Different pixel centerings were used for each artificial star, and the pixel centering varied slightly from frame-to-frame as in the real data. Poisson statistics were used to add errors in the artificial stars using an assumed gain of 14 electrons/DN. These frames were then run through the photometry routines identical to those discussed in Sec. *2.1*. This was done 23 separate times with different brightnesses chosen for the artificial stars each time.

For each of the artificial star runs, the final list from the photometry procedure was compared with the input list of artificial stars, and also with the final photometry list from the original frames. An artificial star was considered to be found if there was a detection within one pixel of the position where the star was placed and if there was no corresponding detection on the original frame. If a match was found with both the artificial star position and with an object on the original frame, the artificial star was considered found if the measured magnitude was closer to the magnitude of the artificial star than to the magnitude of the star on the original frames. This properly accounts for incompleteness due to crowding as well as from incompleteness due to detection efficiency of faint stars above the background.

The artificial stars also provided an estimate of the photometric errors, at least for the fainter stars. A limitation of the artificial stars is that they are reduced with the same PSF

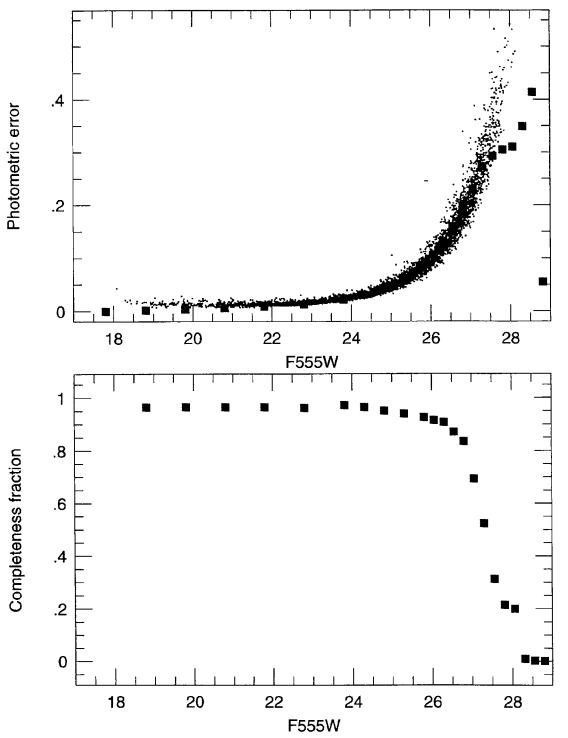

FIG. 3. Top panel: error estimates returned by the profile-fitting routine (small points) and the observed rms errors of the artificial stars (large points). Bottom panel: completeness as inferred from the artificial star experiments.

that is used to create them, so there are no errors resulting from inaccuracies in the PSF models. Such errors dominate for brighter stars, so the artificial stars cannot be used to judge the photometric errors for such stars. However, for all but the brightest stars, PSF errors are small compared with errors arising from Poisson statistics and readout noise, so the artificial stars provide good error estimates. At each artificial star brightness, we tabulated the errors for each artificial star in both F555W and F814W. The errors include systematic errors which arise from crowding (in which magnitudes in both colors are usually affected in the same direction), as well as random error from Poisson statistics (independent in each color). The artificial star tests also accurately reveal the bias in the faintest stars which arises from the fact that only positive noise fluctuations are detected at the faintest levels. The tables of observed errors in the artificial stars were saved for use with the generation of artificial color-magnitude diagrams and luminosity functions discussed below.

The measured completeness and random error estimates are shown in Fig. 3. The top panel shows the rms errors observed for the artificial stars (large points) and the errors returned by the PSF fitting routine for the real stars as a function of magnitude. The observed errors are larger than those predicted by the artificial stars for the brightest stars, as expected because a perfect PSF was used to reduce the artificial stars. At intermediate brightness, the errors for the artificial stars are slightly larger than those estimated for the true stars, but this may be caused by the fact that the rms values for the artificial stars are contaminated by some measurements with systematic errors because of crowding. For the faintest stars, the rms errors of the artificial stars are significantly lower than the error estimates for the real stars. This is caused by the fact that only the positive noise fluctuations are detected as stars at these levels, thus artificially reducing the measured scatter, since the rms values are computed only from stars which were detected. The lower panel shows the completeness as inferred from the artificial stars; note, however, that this completeness curve cannot be applied directly to the raw data because it does not include the systematic photometric errors which are present at the faintest magnitudes.

At the faintest magnitudes, the artificial star tests are difficult to interpret accurately because of the effect of digitization in the WFPC2 electronics. Unfortunately, the current data set was taken with a gain of 14 electrons/DN (an oversight on our part), so digitization effects can be severe for the faintest stars. The effect of digitization depends on the exact value of the background sky level and the brightness of the stars. Consequently, we do not fully trust our completeness tests at the faintest magnitudes, and in our fits to the luminosity function, we only consider stars for which we conservatively feel that we have good completeness and error estimates; namely, stars with $M_{F555W} \lesssim 26.3$.

An estimate of the number of spurious detections is of equal importance to an understanding of the completeness for the measurement of a luminosity function. However, estimating the number of spurious detections is more difficult. We have attempted to minimize the number of spurious detections in several ways: (1) we have inspected the images before the photometric reduction and masked out regions with detector flaws and regions which contain background galaxies, (2) our star finding threshold is relatively high, $\gtrsim 5\sigma$, so we should not be detecting noise peaks, and (3) we use a conservative limit on goodness-of-fit for accepting objects for which we perform photometry. Visual inspection shows that we do not appear to have a large number of spurious detections remaining after these techniques are applied; in subsequent analysis, we make no effort to correct for the few which have survived, since we cannot determine a reasonable estimate for the number of spurious detections as a function of apparent magnitude.

3. MODELS

Astrophysical interpretation of the observed color-magnitude diagram and luminosity functions require models of stellar evolution as well as estimates of the distance and extinction to the observed field.

3.1 Isochrones

We have chosen to primarily use the models recently published by the Padua group (Bertelli *et al.* 1994; Bressan *et al.* 1993; Fagotto *et al.* 1994a,b). These models use the most recent set of radiative opacities (OPAL) from the Livermore group (Rogers & Iglesias 1992; Iglesias *et al.* 1992). Also, they attempt to include evolution throughout the entire stellar lifetime for stars of a wide range of mass, although in this

work we are mostly interested only in the main sequence evolution. The models are available for a range of metallicities from $Z = 0.0004$ to $Z = 0.05$. The stellar evolution models include convective overshoot, which leads to longer inferred main-sequence lifetimes as compared with models which do not include this effect.

One possible limitation of these tracks is that solar abundance ratios for the heavy elements are assumed at all metallicities. Another limitation is that only stars with $M \geq 0.6$ $M_\odot$ are given. This is a concern even for extragalactic studies in nearby galaxies because *HST* allows observations of faint stars. A star of 0.6 $M_\odot$ has an approximate absolute magnitude of $M_V \sim 7-8$, depending on the metallicity. This corresponds roughly to an apparent magnitude of $\sim 26-27$ in the LMC; this is similar to the brightness of our faintest stars. To extend the isochrones to lower mass stars, we have used the stellar models of Bergbusch & Vandenberg (1992) for low metallicities and Swenson *et al.* (private communication) for higher metallicities. These do not match the Padua isochrones because of different opacities and abundance ratios (the Bergbusch and Vandenberg isochrones include oxygen enhancement), but we force a match by adjusting the effective temperatures and luminosities for stars of 0.6 $M_\odot$; for lower masses the Bergbush and Vandenberg and Swenson isochrones are shifted by the constant offset in $\log T_e$ and $\log L$ derived for the 0.6 $M_\odot$ stellar models. Clearly, this is only an approximation for the lower mass stars, but since they represent only a minute fraction of our sample, we expect that it does not introduce severe errors in the interpretation.

In subsequent sections, whenever isochrones are compared directly with the data, we have chosen parameters (metallicity and age) which are tabulated in the above references, i.e., we have not used any interpolation. However, in the construction of our model color-magnitude diagrams and luminosity functions, we need to use arbitrary choices of age. The isochrones for ages that are not tabulated were determined by resampling each of the tabulated isochrones into 100 equally spaced mass points within each of 9 distinct evolutionary stages. For any desired age the resampled isochrones were then interpolated point by point to get a new set of masses, effective temperatures, and luminosities. Splitting the isochrones into equivalent evolutionary stages ensures that the correct shape of the isochrones is preserved during interpolation.

We also need to transform the theoretical isochrones into the observational plane. To do so, we used the set of model atmospheres from Kurucz (1993) and the filter bandpasses for the WFPC2 system as defined by H95B. We first computed WFPC2 colors for all of the Kurucz atmospheres. For each star in each isochrone, we then interpolated in the color tables to get the appropriate colors for the stellar effective temperature, metallicity, and surface gravity. The Kurucz atmospheres are probably a poor match to real stars with temperatures $\lesssim 4000$ K, but our data have very few stars this cool.

3.2 The IMF

In subsequent sections, we discuss constraints on the IMF imposed by the observations. We will assume that the IMF is well represented by power law relations. In addition to solving for an IMF slope , we consider ''standard'' IMFs of two forms: (1) a Salpeter IMF, with $dN/dM \propto M^{-2.35}$ over the entire mass range, and (2) the recent IMF determination in the solar neighborhood by Kroupa *et al.* (1993), who give $dN/dM \propto M^{-2.7}$ for $M > 1$ $M_\odot$, $dN/dM \propto M^{-2.2}$ for $0.5 > M > 1$ $M_\odot$, $dN/dM \propto M^{-1.3}$ for $M < 0.5$ $M_\odot$. We note that over the mass range spanned by our observations, $0.6 \lesssim M \lesssim 3$ $M_\odot$, a Salpeter slope is a reasonable match to the Kroupa, Tout, and Gilmore IMF.

Whenever we fit for an IMF slope, the fit is for a single power law over the observed range of stellar masses.

3.3 Distance and Reddening

We have adopted a distance modulus of 18.5 for the LMC field (see Feast 1991). This probably has uncertainties of ± 0.1 mag. For the extinction, we have adopted a foreground extinction of $E(B-V) = 0.07$ mag (Schwering & Israel 1991). We have arbitrarily adopted an additional reddening of $E(B-V) = 0.03$ mag for internal extinction within the LMC. The reddenings have been converted to extinction in the WFPC2 filter system using the data presented in H95B. Uncertainties in the total reddening are likely to be within a few hundredths of a magnitude, implying only relatively small errors in derived ages for younger populations.

3.4 Simulations

To compare observations with models which include a mix of stellar populations and incorporate knowledge of the observed errors (random and systematic), we simulate color-magnitude diagrams based on isochrones, assumed star formation histories, and observed errors. The inputs to the simulation include the slope of the IMF, the fraction of stars considered to be binaries, and any number of star formation epochs, defined by a start and end epoch, a relative strength of star formation during the epoch, and a metallicity. For binary stars, each star is assumed to be drawn independently from the IMF, with uncorrelated masses.

The simulation software loops over each star formation epoch, interpolates to get isochrones at many different discrete ages within this epoch, randomly draws stars using the desired IMF, and determines the intrinsic color and brightness of each star. Another random number determines whether the star is a binary, and if so, another star is chosen randomly from the IMF and the brightnesses of the two stars are combined. An apparent magnitude is then computed based on the distance and extinction. The star is either considered detected or rejected, depending on the detection probability as determined from the completeness histograms from the artificial star tests. If detected, an observed error for the star is randomly drawn from the artificial star results. Enough stars are simulated so that counting statistics in the model color-magnitude diagram are negligible. The output is a color-magnitude diagram or a luminosity function which can be directly compared with the observations.

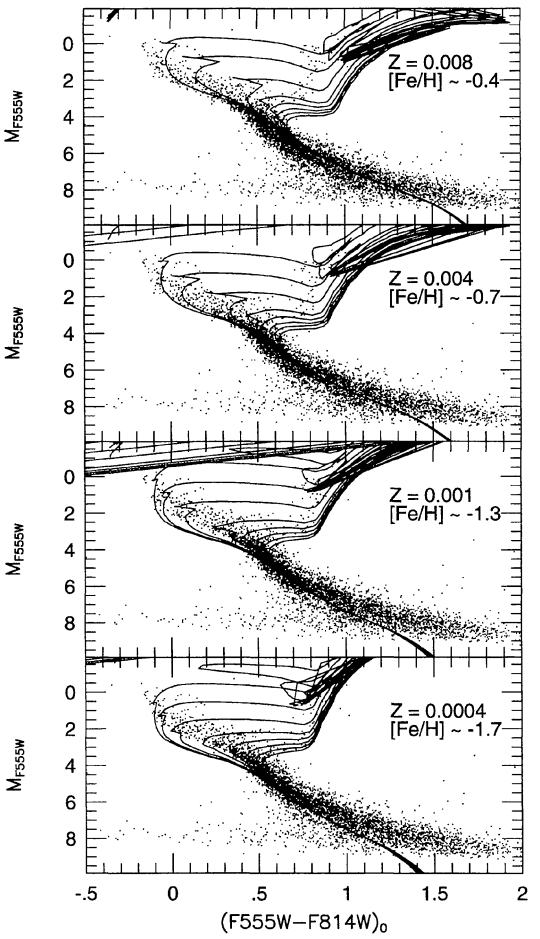

FIG. 4. The color-magnitude diagram after correction for distance, extinction, and reddening. The four panels overlay four different sets of stellar isochrones, with metallicites Z = 0.0004, 0.001, 0.004, and 0.008. Isochrones for ages of 0.5, 1, 2, 4, 6, 8, 10, and 12 Gyr are shown.

4. RESULTS

4.1 Stellar Population Components

Figure 2 shows a well-defined main sequence and a giant branch. The upper main sequence is significantly broader than expected from observational errors. There is a definite main sequence turnoff around $M_{F555W} \sim 3.5$ and a strong suggestion of another turnoff around $M_{F555W} \sim 2.5$ (with subgiant branches roughly 0.5 mag brighter). Figure 4 plots the same data along with isochrones for several different metallicities: Z = 0.008, 0.004, 0.001, and 0.0004 ([Fe/H] ~ -0.4, -0.7, -1.3, -1.7). In each plot isochrones are shown for ages 0.5, 1, 2, 4, 6, 8, 10, and 12 Gyr.

First, we consider the upper main sequence. As discussed in Gallagher *et al.* (1996), stars in this region of the color-magnitude diagram spend roughly half their lives within 0.3 mag of the ZAMS before becoming brighter. Gallagher *et al.* show that the observed distribution of stars along single evolutionary tracks in the upper part of the color-magnitude diagram is roughly consistent with the amount of time stars spend at each location, implying roughly constant star formation over the last few billion years. There is a concentration of stars on the blue edge of the main sequence, and we adopt the blue edge as the empirical ZAMS. If the stellar models are accurate, then we derive a metallicity of the upper main sequence stars of somewhere between $Z=0.004$ ([Fe/H]$=-0.7$) and $Z=0.008$ ([Fe/H]$=-0.4$). This is comparable to other measurements of the metallicities of bright LMC stars (Da Costa 1991).

The location of the lower main sequence suggests that at least some of the low mass stars have lower metallicities than the stars on the upper main sequence; isochrones of a single metallicity are unable to fit both the upper and lower sequence simultaneously. Assuming the isochrones are accurate, there must be a significant component of stars with $0.001<Z<0.004$. The width of the lower main sequence around $M_{F555W}\sim 5$ is broader than expected from observational errors, suggesting that there is a spread in metallicity, although binaries may also contribute to the observed spread.

The faintest main sequence turnoff occurs around $M_{F555W}\sim 3.5$. The age we infer is dependent on the metallicity of the population which is in the process of evolving off the main sequence at this point. For the metallicities derived for the upper main sequence, an age of roughly 6 Gyr is inferred. However, if the population is metal-poor, an age of $\geqslant 10$ Gyr is inferred.

There is tantalizing evidence of a second main sequence turnoff around $M_{F555W}=2.5$ with a subgiant branch around $M_{F555W} = 2$. As discussed in Gallagher *et al.*, this would represent an epoch with enhanced star formation. The inferred age for this "burst" is between 2 and 4 Gyr depending on the assumed metallicity. However, with observations only in this single field, it is impossible to know if this represents a global or a local increase in star formation rate.

At first glance, the location of the giant branch suggests that the metallicity of the evolved population is low. The giant branch is quite blue and the only isochrones that fall as blue are the lowest metallicity set with $Z=0.0004$ ([Fe/H] $=-1.7$). A similar conclusion is reached if one compares the data with *HST* data of old Galactic globular clusters (H95B) or if one transforms the observed WFPC2 colors to $V-I$ and compares with the empirical giant branches presented by Da Costa & Armandroff (1990), so this is not a calibration problem or a conclusions which depends on the accuracy of the stellar models.

However, it is possible that the blue giant branch arises from a relatively young population. The stellar models suggest that young stars ($\sim$ 1 Gyr) could populate a blue giant branch brighter than $M_{F555W} = 1$. For $1<M_{F555W}<2$, the giant branch could be populated by stars with metallicities around $Z = 0.001$ with ages of a few Gyr. In this scenario, only the lowest part of the giant branch would need to be populated by old, very metal poor stars.

4.2 The Luminosity Function

Figure 5 shows the observed luminosity function from the F555W band. Both the uncorrected and a completeness-corrected luminosity function are shown, although the completeness correction applied here does not include any cor-

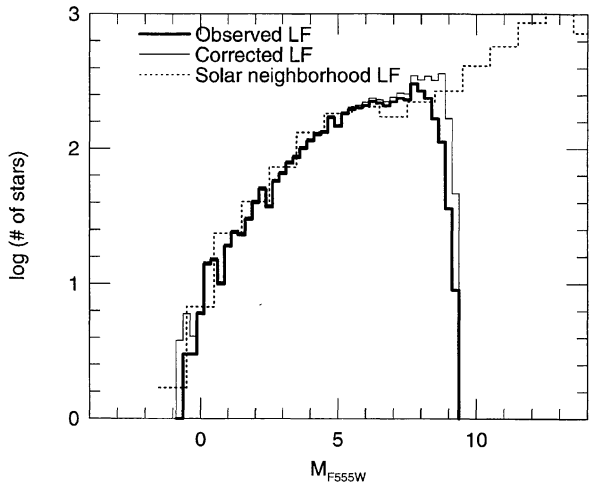

FIG. 5. The observed luminosity function with no correction (bold line), and with a correction for incompleteness (light line). The solar neighborhood luminosity function from Wielen *et al.* (1983) is shown with a dotted line.

rection for the systematic photometric errors which occur at the faint end. In subsequent discussion, we consider only the luminosity function brighter than $M_V \sim 7.5$.

In general the luminosity function looks relatively smooth. For comparison, we also show the solar neighborhood luminosity function from Wielen *et al.* (1983), with arbitrary normalization. They are roughly comparable, but it appears that the LMC field may have a surplus of lower mass stars or a deficiency of higher mass stars as compared with the solar neighborhood.

Of some interest is the flattening which occurs around $M_{F555W} \sim 7$, which corresponds to the so-called Wielen dip in the solar neighborhood luminosity function. This dip is likely to be caused by structure in the mass-luminosity relation rather than in the mass function (e.g., Kroupa *et al.* 1993), and if so, it is probably metallicity dependent. In fact, our model luminosity functions show such an effect, with a larger dip at higher metallicities. Given the observed dip, these models suggest that the dominant population around $M_{F555W} \sim 7$ is not very metal-poor.

4.3 The IMF

The IMF is best constrained using the lower main sequence because the effects of evolution are minimized for low mass stars. However, even low mass stars evolve in luminosity over several billion years, so a derived IMF is not completely insensitive to the star formation history. In addition, the luminosity function also depends on metallicity (since metallicity affects the mass-luminosity relation) and on the assumed binary fraction.

To test the sensitivity of the derived IMF to these various parameters, we did a series of comparisons of model luminosity functions with the observed LF. We tried models for 3 choices of a star formation history, namely, populations with stars that were either exclusively young (0–3 Gyr), intermediate (3–6 Gyr), or old (6–12 Gyr). We also used two possible choices of metallicity ($Z = 0.008$ and 0.001), and two choices of binary fraction (0.5 and 0.0). All of the model luminosity functions were constructed by simulation which includes the effects of both random and systematic photometric errors (as inferred from our artificial star tests).

TABLE 1. 95% confidence limits on IMF slopes from lower main sequence.

Start lookback time (Gyr)	End lookback time (Gyr)	Z	Binary fraction	IMF slope
3	0	0.008	0.5	$-2.74 > \alpha > -3.08$
6	3	0.008	0.5	$-2.58 > \alpha > -3.02$
12	6	0.008	0.5	$-2.04 > \alpha > -2.68$
3	0	0.001	0.5	$-2.56 > \alpha > -2.88$
6	3	0.001	0.5	$-2.24 > \alpha > -2.66$
12	6	0.001	0.5	$-1.64 > \alpha > -2.12$
3	0	0.008	0.0	$-2.58 > \alpha > -2.98$
6	3	0.008	0.0	$-2.40 > \alpha > -2.92$
12	6	0.008	0.0	$-1.74 > \alpha > -2.50$
3	0	0.001	0.0	$-2.28 > \alpha > -2.68$
6	3	0.001	0.0	$-1.94 > \alpha > -2.46$
12	6	0.001	0.0	$\alpha > -1.76$

We compared the observed and model LFs using a Kolmogorov–Smirnov test, which can be used to disprove the hypothesis that the model and observed functions come from the same parent distribution. Using the KS test properly accounts for counting statistics in the observed LF and allows a comparison without binning the data. However, one does need to consider the magnitude limits over which the comparison is performed. If one compares distributions over a large magnitude range, this makes the inferred IMF more sensitive to the star formation history. However, as one limits the magnitude range of the comparison, counting statistics weaken the significance of the results.

After some experimentation, we chose to do the comparison in the magnitude range $4 < M_{F555W} < 7.5$. The bright end was chosen to lie fainter than the oldest turnoff, and the faint end was chosen to be the faintest magnitude where we feel that our completeness and systematic errors are well understood. This magnitude range corresponds to a mass range from ~ 1.1 to ~ 0.6 solar masses.

The results from these comparisons are shown in Table 1, in which we present the 95% confidence limits on the IMF slope (α) of the LMC population. Similar results are obtained when one fits the F814W luminosity function instead of the F555W LF. The data for the observed and several model luminosity functions are shown in Fig. 6. The three different panels are for three combinations of star formation history and metallicity, and a range of model IMFs is shown on each plot.

Inspection of the KS results shows that the derived IMF from our chosen magnitude range is relatively insensitive to age for younger populations. Older than 6 Gyr, main sequence evolution becomes important and steeper luminosity functions are predicted by the model, leading to an flatter inferred IMF. The relatively large sensitivity to star formation history, at least between a predominantly old and predominantly young population, was surprising to us, but it is confirmed upon inspection of analytical luminosity functions derived from the stellar models. Figure 7 shows model luminosity functions for ages of 1 and 12 Gyr for $Z = 0.008$, and

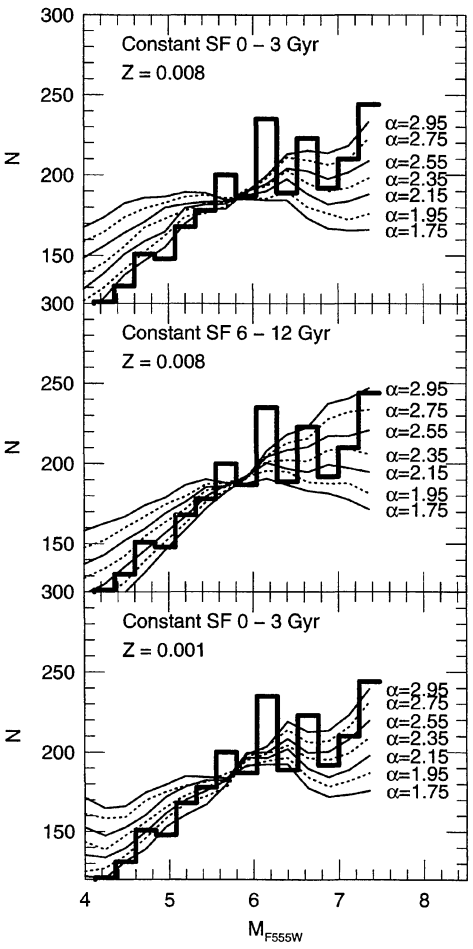

FIG. 6. The observed luminosity function of stars with $4<M_{F555W}<7.5$ (bold lines), along with simulations from model luminosity functions for different assumed IMF slopes (α). The three panels show model results for different choices of star formation history or metallicity.

it is clear that the older population has a significantly steeper luminosity function, even at magnitudes *fainter* than the turnoff. To determine an IMF slope completely independently of the star formation history requires observations of stars fainter than $M_{F555W} \sim 7$.

The derived IMFs are steeper for higher metallicities, but not by a very large amount. The assumed binary fraction also has a small effect, leading to a slightly steeper IMF for a higher binary fraction.

The most conservative limits on the IMF slope without any assumptions about the star formation history or metallicity give a slope (95% confidence limits) between -1.6 and -3.1. However, because the field has an upper main sequence, it is clear that the population is not entirely old, and more reasonable limits are -2.0 and -3.1. In this range, the steeper values are required when the population is more metal rich and younger. The inferred values are consistent with the Salpeter value (-2.35) and marginally consistent with the value from Kroupa, Tout, and Gilmore appropriate to this mass range (-2.2), although the preferred values are slightly steeper than either for most reasonable choices of metallicity and star formation history.

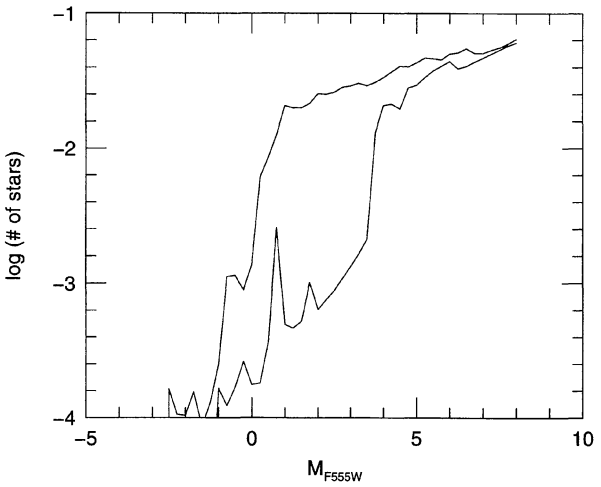

FIG. 7. Semi-analytical model luminosity functions for two choices of population age, 1 and 12 Gyr, for $Z = 0.008$. Note the slope difference in the LF even at magnitudes fainter than the turnoff.

4.4 Star Formation Histories

Given some constraints on the IMF from the lower main sequence, we can use the measured luminosity function over the entire observed magnitude range to constrain star formation histories. Ideally, one would use color information as well as brightness and fit the Hess diagram rather than just the luminosity function, but experimentation has shown that this method is difficult to implement because of the unknown age-metallicity relation, the relatively few number of stars we have to fit in some regions of the color-magnitude diagram, and uncertainties in the stellar evolution and atmosphere models. Instead, we use the color-magnitude diagram to suggest plausible components for a model of the star formation history, and then attempt to fit the luminosity function using these components. We begin by considering models with a Salpeter IMF.

First, we consider whether the observed luminosity function is consistent with the history of star formation favored by Bertelli *et al.* (1992) and others, namely a low star formation rate until $\sim$ 4 Gyr ago. Figure 8 shows model luminosity functions for a model which has a constant, low star formation rate from 15 Gyr to a "burst time," τ_B, and then a tenfold increase in star formation rate from τ_B to the present. Bertelli *et al.* derived a preferred value of $\tau_B \sim 4$ Gyr for a field nearby to our field, although they found acceptable values between 2 and 5 Gyr. Note that their preferred model has about four times as many young stars as old stars (where the distinction between young and old is drawn at τ_B). In our models, a Salpeter IMF is used for all epochs of star formation (same as Bertelli *et al.*), and a binary fraction of 0.5 is assumed.

Figure 8 shows three models: in each model, $\tau_B = 4$ Gyr and the young stars have $Z = 0.008$, but the models differ in that the older stars have $Z = 0.008$, 0.001, and 0.0004. The left panels in this and subsequent figures show the observed luminosity function (histogram), the model luminosity func-

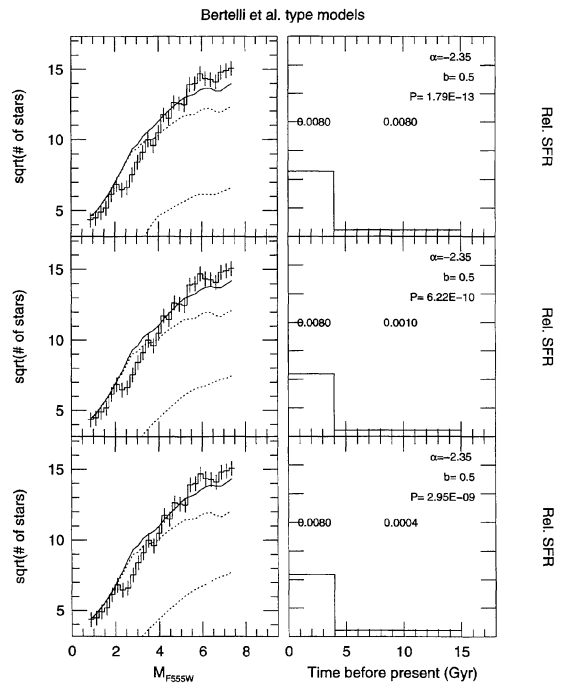

FIG. 8. Comparison of observed luminosity function with a simulation from models with the star formation history preferred by Bertelli *et al.* (1992). The left panels show the observed LF (histogram) and the model LF (solid line). Individual components of the LF are shown with dotted lines. The right panels schematically show the star formation history of the model. The text in the right panels gives the metallicity of each component, the assumed IMF slope (α), the binary fraction (b), and the probability (P) that the deviation between the model and the data is as large as observed under the null hypothesis that the distributions are the same.

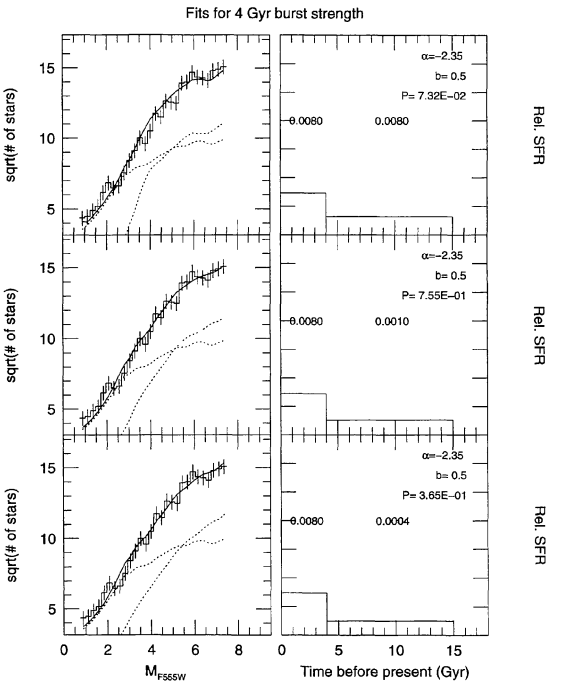

FIG. 9. Same as Fig. 8 but for models in which the strength of the 4 Gyr burst is a free parameter.

tion after normalizing the model to have the same number of stars as the observed luminosity function (solid line), and the various components of the model luminosity function (dotted lines). The square root of the number of stars is plotted so that the error bars due to counting statistics have the same apparent amplitude in all bins. The right panels schematically show the relative star formation rates in the model and give the metallicity in each epoch of star formation, as well as the assumed IMF slope (α) and binary fraction (b), which are assumed to be time-independent. We also show the probability (P) that the deviation between the model and the data is as large as observed under the null hypothesis that the distributions are the same.

From the color-magnitude diagram, we expect that the older stars have a lower metallicity than the younger stars because the lower main sequence is bluer than expected for the metallicity of the upper main sequence. However, we find that none of these models adequately fit the observed luminosity function, regardless of the assumed metallicity. There are too many lower main sequence stars relative to upper main sequence stars to fit models with such a strong increase in star formation rate. The agreement is slightly better for a binary fraction of 0.0, but the same systematic deviations are seen.

If we wish to keep a star formation history of the same qualitative form, the increase in star formation rate at 4 Gyr must be more modest. Figure 9 shows similar models allowing the increase in star formation rate to be a free parameter in a least squares fit to the binned data. This shows that acceptable fits can be obtained with a threefold increase in star formation rate at 4 Gyr. If star formation started in the LMC at a lookback time of 12 Gyr instead of 15 Gyr, the corresponding rate increase at 4 Gyr would be even less. Note that in such models, there are about the same number of old stars as young stars.

Although these models provide statistically acceptable matches to the data, they all appear to predict slightly too few stars with $1 < M_{\mathrm{F555W}} < 2$, and slightly too many stars with $3 < M_{\mathrm{F555W}} < 4$ (fainter for $Z = 0.008$), or, in other words, the observed luminosity function is shallower than the models for stars with $M_{\mathrm{F555W}} \lesssim 4$. This suggests that there are too many intermediate age stars in the models. We note that the problem is worse if we adopt the Kroupa *et al.* IMF, since this has a *steeper* slope in this region of the color-magnitude diagram. To attempt to rectify this, we consider a three-epoch star formation history, motivated by the age distribution of clusters in the LMC. Figure 10 shows fits for star formation rates in three epochs: 12–10, 10–4, and 4–0 Gyr. These fits are still not much better than the two epoch fits. However, the discrepancies can be reduced by allowing τ_B to decrease. Models with $\tau_B = 2,3,4$ Gyr are shown in Fig. 11. The model with $\tau_B = 2$ Gyr provides an excellent match to the data.

All models considered so far which provide a reasonable match to the luminosity function with a Salpeter IMF have star formation rates which only vary by a factor of a few. These models have at least a comparable number of old stars (age greater than 4 Gyr) and young stars. This star formation

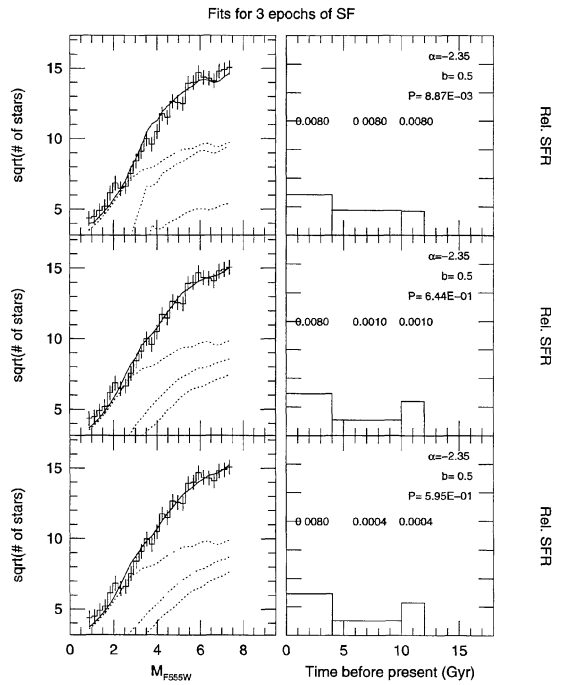

FIG. 10. Same as Fig. 9 but for models with three separate epochs of star formation.

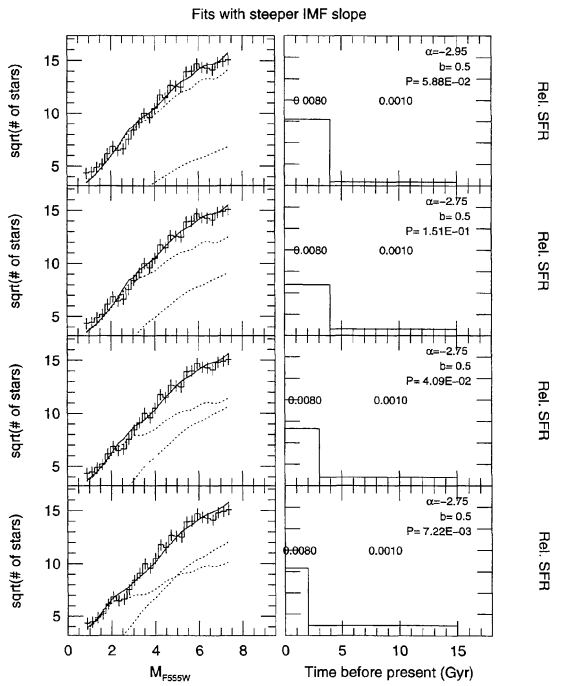

FIG. 12. Same as Fig. 9 but for models with steeper IMF slopes.

scenario differs significantly from that suggested by previous studies which find that the bulk of the field stars in the LMC are young.

It is possible, however, to get models with a stronger increase in star formation rate (and hence more young stars) to fit the data if we allow the IMF to be steeper. Figure 12 shows the luminosity function fits for IMF slopes of -2.75 and -2.95 allowing for the rate increase to be a free parameter (top two panels). For clarity, only models with $Z = 0.001$ at early times are shown. These IMFs are among the steepest allowed from the lower main sequence. These models are marginally consistent with the data. They cannot be improved by choosing a different burst epoch because models with smaller τ_B predict too many faint stars (bottom panels). Models with mostly young stars also would require the metallicity to evolve rapidly from moderately low values at τ_B to the current present value in order to match the locus of points on the color-magnitude diagram.

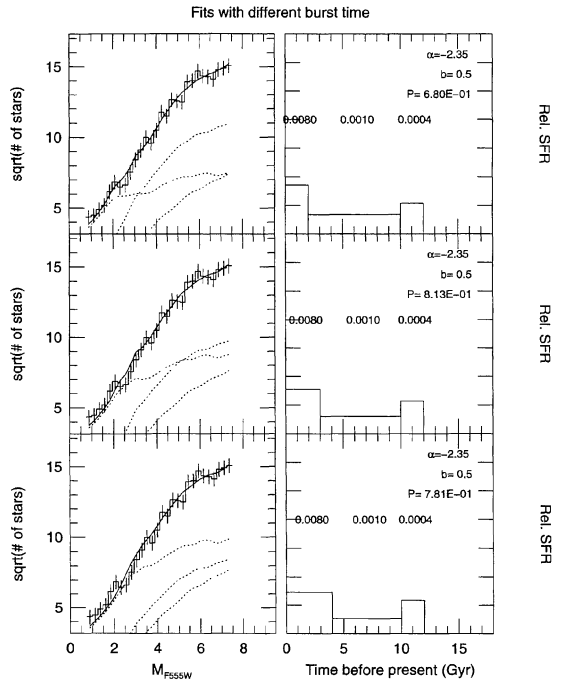

FIG. 11. Same as Fig. 10 but for models with different τ_B.

While we are considering variations in the IMF, we also consider the effect of adopting the Kroupa *et al.* IMF in Fig. 13. This IMF is steeper for the brighter stars than the Salpeter value, and slightly shallower for fainter stars. Fits with $\tau_B \sim 2$ Gyr are statistically acceptable although they do not provide as good a match as a Salpeter IMF.

So far, we have ignored the 2 Gyr burst noticed by Gallagher *et al.* (1996). As noted by Gallagher *et al.*, however, the relative number of stars in this burst must be fairly small because no large discontinuities are seen in the luminosity function at a magnitude corresponding to the turnoff of a 2 Gyr population. Gallagher *et al.* suggest that the subgiants seen around $M \sim 2$ can be explained by a threefold increase in star formation rate for a period of 0.1 Gyr. With our models, this burst event would contribute $\lesssim 15\%$ of the total number of stars with ages less than 4 Gyr, and consequently, including the event would not significantly alter conclusions based on models which do not include the burst component.

It is clear that we have not fully explored the available parameter space and it is likely that variations on the above

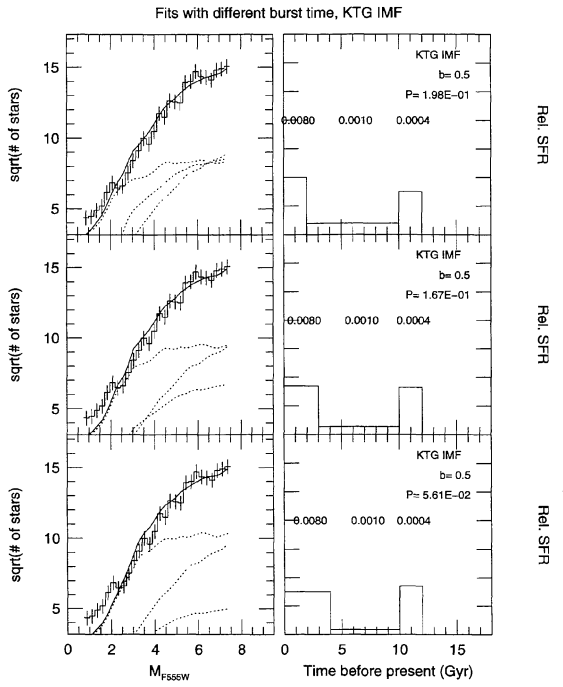

FIG. 13. Same as Fig. 11 but for models with the Kroupa *et al.* IMF slopes.

models could provide equally good fits. Significantly more data would be needed to draw distinctions between more subtle model differences. From analysis of the current luminosity function, we adopt as our best model a star formation history with 3 epochs of star formation: constant star formation rate (SFR) between 12–10 Gyr, a slight decrease in SFR from 10–2 Gyr, and a factor of 2–3 increase in SFR between 2 Gyr and the present (Fig. 11, top panel). This model uses a Salpeter IMF at all epochs. In addition, one might include a 0.1 Gyr long burst 2 Gyr ago at three times the recent star formation rate to give the $M_{F555W} \sim 2$ subgiant branch.

This model has roughly the same number of old stars as young stars, in contrast to previously suggested models of star formation in the LMC. A large relative number of young stars has previously been suggested by the shape of the main sequence luminosity function (e.g., Butcher 1977) and by the relative number of upper main sequence and giant stars (e.g., Bertelli *et al.* 1992). Our main sequence luminosity function, however, cannot be fit with a dominant component of young stars unless the IMF slope is steeper than the Salpeter value. The reason that our results are different from those inferred by Bertelli *et al.* is not clear, although those results are based on observations of the giant branch and upper main sequence (and consequently depend on stellar models of giant and post-giant branch evolution), whereas our results are derived predominantly from observations of the main sequence.

To determine whether our model predicts too many giants, we simulated a color-magnitude diagram. The comparison of our model color-magnitude diagram with the observed diagram is shown in Fig. 14, with the observed diagram on the left and our best model on the right. The model has slightly more giants than are observed in this field, but the total numbers are small so counting errors are large. The

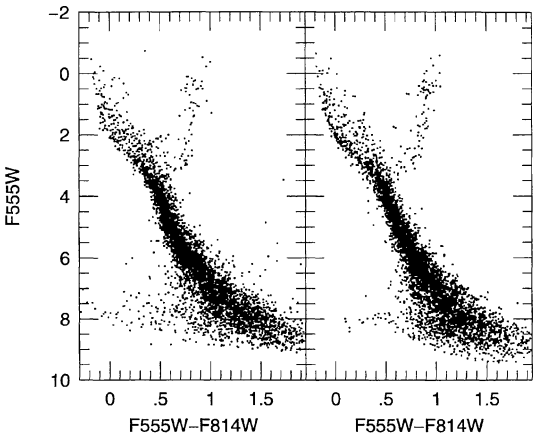

FIG. 14. The observed color-magnitude diagram (left) along with a simulated color-magnitude diagrams of our preferred model (right).

model might be better constrained using ground-based data which sample many more stars. However, one must also consider possible errors in the evolutionary models for giant and post-giant branch stars.

There are some minor problems apparent in our color-magnitude diagram simulation. The width of the upper main sequence is narrower in the model than in the data. This suggests that an exactly constant star formation rate over the past 2 Gyr is not correct. The observation that the upper part of the main sequence in the observed color-magnitude diagram shows little concentration towards the blue side suggests that the star formation rate in the past Gyr may have been slightly declining; this would give a more uniform distribution of stars in color. However, we have too few stars in this region to attempt a more detailed model. We can also see that the main sequence is too smeared out in the model around $3 < M_V < 4$. This results from incorporating stars of age 2 Gyr at two discrete metallicities, $Z = 0.008$ and $Z = 0.001$, in the model. The lower metallicity stars add a bluer and brighter sequence. This disagreement can be reduced by raising the metallicity of the middle epoch, and by implementing a more smoothly varying age-metallicity relation. An additional problem is that we find that it is difficult to get giant branches quite as blue as observed using our model and the current stellar isochrones. Some or all of these problems could be eliminated by subtle adjustments in model parameters, but we do not feel that we have sufficient data to warrant such fine tuning, given the likely uniqueness problems and possible small errors in the stellar models.

5. SUMMARY

We have investigated the initial mass function and the star formation history in an outer LMC field based on *HST* imaging which provides accurate photometry down to $V \sim 26$. We use the luminosity function of stars which are fainter than the oldest turnoff to determine constraints on the IMF. We find that even for these stars, which have masses $0.6 < M < 1.1\ M_\odot$, the derived IMF depends on the assumed star formation history and metallicity, though not as much as

for more massive stars. We derive IMF slopes which are consistent with the Salpeter value or the value derived for the solar neighborhood, although for most reasonable choices of star formation history, our derived slopes are slightly steeper than these values. We can conservatively rule out IMF slopes shallower than -1.6 and steeper than -3.1; for plausible star formation histories the limits are -2.0 and -3.1.

Using a Salpeter IMF, we have investigated the star formation history in our field using the observed luminosity function. We find that a model of star formation for the LMC suggested by previous studies, namely that the majority of field stars are younger than 4 Gyr, cannot fit our observed luminosity function; there are too many faint main sequence stars compared to the number of bright stars. We find that we can get acceptable fits if the star formation rate increases mildly a few billion years ago, leading to a model which has roughly comparable numbers of stars older and younger than 4 Gyr. Our best model has a star formation rate which is roughly constant for 10 Gyr, then increases by roughly a factor of 3 and remains constant at that level until the present time. Simulated color-magnitude diagrams of this model provide a reasonable match to the observed color-magnitude diagram as well as to the observed luminosity function.

Alternatively, we can fit the luminosity function with a predominantly young population if the IMF has a steeper slope than the Salpeter value.

Data on additional fields in the LMC is in the process of being obtained and analyzed, and these data should help to determine whether the star formation history derived from the current field is representative of the LMC as a whole. If the luminosity functions in all fields are similar, they can be combined and provide stronger constraints on the details of the IMF and star formation history in the LMC.

This work was supported in part by NASA under contract NAS7-918 to JPL.

REFERENCES

Bergbusch, P. A., & Vandenberg, D. A. 1992, ApJS, 81, 163
Bertelli, G., Mateo, M., Chiosi, C., & Bressan, A. 1992, ApJ, 388, 400
Bertelli, B., Bressan, A., Chiosi, C., Fagotto, F., & Nasi, E. 1994, A&AS, 106, 275
Bressan, A., Fagotto, F., Bertelli, G., & Chiosi, C. 1993, A&AS, 100, 647
Butcher, H. 1977, ApJ, 216, 372
Da Costa, G. S., & Armandroff, T. E. 1990, AJ, 100, 162
Da Costa, G. S. 1991, AJ, 100, 162; in The Magellanic Clouds, IAU Symposium 148, edited by R. Haynes and D. Milne (Kluwer, Dordrecht), p. 183
Fagotto, F., Bressan, A., Bertelli, G., & Chiosi, C. 1994a, A&AS, 104, 365
Fagotto, F., Bressan, A., Bertelli, G., & Chiosi, C. 1994b, A&AS, 105, 29
Feast, M. W. 1995, in Stellar Populations, IAU Symposium 164, edited by P. C. Van Der Kruit and G. Gilmore (Kluwer, Dordrecht), p. 153
Feast, M. W., 1991, in New Aspects of Magellanic Clouds Research, edited by B. Baschek, G. Klare, and J. Lequeux (Springer, Berlin)
Gallagher, J. S., *et al.* 1996, ApJ, 466, 732
Guhathakurta, P., Yanny, B., Schneider, D. P., & Bahcall, J. N. 1996, AJ, 111, 267
Holtzman, J. A. 1997, in preparation
Holtzman, J. A., *et al.* 1995a, PASP, 107, 156 (H95A)
Holtzman, J. A., Burrows, C. J., Casertano, S., Hester, J. J., Trauger, J. T., Watson, A. M., & Worthy, G. 1995b, PASP, 107, 1065 (H95B)
Hunter, D. A., Light, R. M., Holtzman, J. A., Lynds, R., O'Neil, E. J., & Grillmair, C. J. 1997, ApJ (in press)
Iglesias, C. A., Rogers, F. J., & Wilson, B. G. 1992, ApJ, 397, 717
Krist, J. E., & Burrows, C. J. 1994, Appl. Opt., 34, 4951
Kroupa, P., Tout, C. A., & Gilmore, G. 1993, MNRAS, 262, 545
Kurucz, R. L. 1993, ATLAS9 Stellar Atmosphere Programs and 2 km/s grid, CD-ROM 13, Smithsonian Astrophysical Journal
Mateo, M. 1991, in The Stellar Populations of Galaxies, IAU Symposium 149, edited by B. Barbuy and A. Renzini (Kluwer, Dordrecht), p. 147
Mateo, M. 1988, ApJ, 331, 261
Olszewski, E. W. 1993, in The Globular Cluster-Galaxy Connection, ASP Conf. Ser. 48, edited by G. Smith and J. Brodie (ASP, San Francisco), p. 351
Rogers, F. J., & Iglesias, C. A. 1992, ApJS, 79, 507
Scalo, J. M. 1986, Fund. Cosmic Phys., 11, 1
Schwering, P. G. W., & Israel, F. P. 1991, A&A, 246, 231
Stryker, L. 1984, ApJS, 55, 127
Vallenari, A., Chiosi, C., Bertelli, G., & Ortolani, S. 1996a, A&A, 309, 358
Vallenari, A., Chiosi, C., Bertelli, G., Aparicio, A., & Ortolani, S. 1996b, A&A, 309, 367
Wielen, R., Jahreiss, H., & Kruger, R. 1983, in Nearby Stars and the Stellar Luminosity Function, IAU Colloquium 76, edited by A. G. Davis Phillip and A. R. Upgren (Davis, Schenectady), p. 163